

Strong-field ionization in particle-in-cell simulations

A.A. Mironov,^{1,*} E.G. Gelfer,^{2,3} I.I. Tupitsin,⁴ M. Jirka,^{2,5} O. Klimo,^{2,5} S. Meuren,⁶ T. Smorodnikova,⁷ R. Taïeb,⁸ S. Weber,² C. Riconda,⁹ M. Grech,⁶ and S.V. Popruzhenko^{10,11}

¹*Center for Theoretical Physics (CPHT), CNRS, École Polytechnique, Institut Polytechnique de Paris, 91128 Palaiseau, France*

²*ELI Beamlines Facility, The Extreme Light Infrastructure ERIC, 25241 Dolni Brezany, Czech Republic*

³*HiLASE Centre, Institute of Physics of the Czech Academy of Sciences, 25241, Dolni Brezany, Czech Republic*

⁴*Department of Physics, St. Petersburg State University, Universitetskaya 7-9, 199034 St. Petersburg, Russia*

⁵*FNSPE, Czech Technical University in Prague, Prague, Czech Republic*

⁶*LULI, CNRS, CEA, Sorbonne Université, École Polytechnique, Institut Polytechnique de Paris, F-91128 Palaiseau, France*

⁷*Stanford PULSE Institute, SLAC National Accelerator Laboratory, Menlo Park, CA 94025, USA*

⁸*Sorbonne Université, CNRS, Laboratoire de Chimie Physique-Matière et Rayonnement, LCPMR, F-75005 Paris, France*

⁹*LULI, Sorbonne Université, CNRS, CEA, École Polytechnique, Institut Polytechnique de Paris, F-75255 Paris, France*

¹⁰*National Research Nuclear University MEPhI, Kashirskoe shosse 31, 115409, Moscow, Russia*

¹¹*Prokhorov General Physics Institute RAS, Vavilova 38, 119991, Moscow, Russia*

We discuss the inclusion of the process of multiple ionization of atoms in high-intensity electromagnetic fields into particle-in-cell (PIC) codes applied to the simulation of laser-plasma interactions. The approach is based on the application of the Perelomov-Popov-Terent'yev formulas for ionization rates within the paradigm of sequential tunnel ionization. We analyze difficulties and possible inconsistencies of the approach, which may cause problems in the implementation of PIC codes. To test the sensitivity to the ionization model variations, we perform simulations of an argon target ionization by an incident high-intensity laser pulse. For this, we implement an original procedure in PIC code SMILEI, which allows us to account for the dependence on the magnetic quantum number in ionization rates consistently, and also include barrier suppression at high fields.

I. INTRODUCTION

In recent decades, particle-in-cell (PIC) simulations have become a pivotal research instrument in the physics of intense electromagnetic fields' interaction with matter [1–3]. Although initially the PIC methods were designed and applied for numerical description of dynamics of fully ionized collisionless plasmas [4–6], the later prominent progress in the code architecture and in the capacity of computer resources has led to a significant expansion of the PIC-based approaches into the physics of many-body classical and quantum systems. The severe restriction on the evolution time of a system simulated by a PIC method still imposes its upper bound on the level of several picoseconds, limiting the scope of consideration by phenomena occurring in the interaction of femto- and attosecond electromagnetic pulses with matter. At the same time, modern PIC codes account for not only the effects of the self-consistent, collective fields but are capable of taking into consideration different elementary processes, which may happen with individual charged particles [2, 3, 6–25].

Here, the characterization “elementary process” stands for any event (beyond a particle push by an electromagnetic field) that involves a few particles, not necessarily all of them true elementary. This includes, in partic-

ular, binary electron-electron, electron-ion and ion-ion collisions [7–10], bremsstrahlung [11–13], Thomson [14–16] and Compton radiation [2, 3, 17, 18, 24, 26, 27], Breit-Wheeler process [2, 3, 17, 18, 24] and ionization of atoms and ions by impact [10] or under the action of the electromagnetic field [2, 6, 19–23]. Cross sections or rates of these processes are known either in the form of exact results or within different approximations. Presently, several PIC codes with essential elementary processes included are being used for simulations of laser-plasma dynamics and radiation in a broad range of parameters. This list includes the codes EPOCH [2, 28], OSIRIS [6], PICADOR [29], PIConGPU [30], SMILEI [31], UMKA [32, 33], WARPX [25]. These codes have already allowed to advance considerably our understanding of laser-plasma interaction under extreme conditions including effects of radiation reaction, production of electron-positron pairs, generation of quantum cascades, excitation of strong magnetic fields and more, see papers [34–36] for the state-of-the-art review.

Difficulties in including elementary processes in PIC simulations stem essentially from the fact that the parameters of plasma and laser fields span giant intervals. In particular and most importantly, typical values of laser intensity vary in the interval $10^{15} - 10^{25} \text{W/cm}^2$, where the lower bound corresponds to the characteristic atomic field where fast ionization and production of multiply charged ions occur, while the upper bound yet remaining out of experimental reach marks the threshold for the generation of quantum cascades of elementary parti-

* Correspondence email address: mironov.hep@gmail.com

cles and other fundamental effects of nonlinear quantum electrodynamics (QED). In many cases, there is no way to provide an analytic quantitatively correct description of a cross-section or rate universally valid in the whole aforementioned interval of intensities so that particular implementations will impose additional restrictions on intensity intervals or other parameters.

In this paper, we analyze the process of field ionization from the viewpoint of its description in PIC codes, particularly, in SMILEI. A quantitatively correct description of the multiple ionization process in the simulation of the plasma dynamics is important for targets made of heavy atoms for several reasons. Firstly, it is required to correctly describe the charge distribution of laser-created plasmas at different stages of the interaction. The concentration of free electrons is one of the key parameters determining the plasma response to intense laser radiation with impact on the plasma formation itself [37], the build-up of sheath fields [38], the overall plasma expansion dynamics [39] or ion acceleration [23, 40]. Secondly, multiple ionization of heavy atoms inside a laser pulse of ultra-high intensity can be used as a specific method of electron injection for their subsequent acceleration [41–44], or to initiate avalanche-type QED cascades [45]. Thirdly, measuring the maximal charge state of heavy ions can be used to determine the peak intensity in the focus of laser pulses delivered by multi-petawatt (PW) facilities. This method tested at lower intensities in [46–48] recently received extended theoretical treatment in view of multi-PW laser diagnostics [49, 50]. These circumstances make a correct inclusion of field-induced ionization in PIC simulation of high demand.

In available PIC codes the process of nonlinear strong-field ionization of multi-electron atoms is realized on the basis of a Monte Carlo algorithm with rates of single-electron ionization described by analytic formulas of Perelomov, Popov and Terent'ev (PPT rates) [51–53], see also reviews [54, 55]. These rates are also known in the literature as ADK rederived by Ammosov, Delone and Krainov in 1986 [56]. Such approximate formulas although applicable in a wide semiclassical domain, can leap out of their range of validity when the simulation parameters change. We analyze situations where such invalidation may happen and compare different implementations of the PPT rates in SMILEI.

The paper is organized as follows. In the next section, we discuss the fundamental constraints on implementations of strong field ionization in PIC codes. Section III is dedicated to the description of specific analytical models of ionization suitable for implementation in PIC codes and analysis of their inaccuracies. Then we describe the numerical implementations of strong field ionization in Section IV and compare the results of PIC simulations for an argon target impinged by a short laser pulse with various models in Section V. Section VI provides the conclusion and outlook of the paper. In Appendix A we discuss the calculation of asymptotic coefficients C_{n^*l} and their impact on ionization rates.

II. FUNDAMENTAL CONSTRAINTS ON A UNIVERSAL DESCRIPTION OF MULTIPLE STRONG FIELD IONIZATION IN PIC CODES

We start from a brief discussion of the most significant constraints imposed on the description of nonlinear strong-field ionization in a PIC code. Technically, it is very difficult to extend the procedure beyond the limits described below. However, there is no need for this for most of the cases of interest. Still, it is instructive to clearly formulate these principal limitations.

- I. The ionization process is assumed of a single-electron nature, without any significant contribution of correlation effects. This means that the electrons are being removed from an atom independently one from another so that the only relevant channel is production of ions A^{n+1} from ions A^n , where n stands for the ion charge state, $n = 0$ for neutral atoms.
- II. For a given charge state, the outermost electron having the lowest ionization potential I_p detaches with the dominant probability, compared to all other electrons so that it is sufficient to account for only this channel.

These two assumptions are well justified only for (i) multiquantum ionization in a field of (ii) sub-relativistic and higher intensity. Condition (i) means that the photon energy of the laser field is small compared to the ionization potential,

$$\hbar\omega \ll I_p . \quad (1)$$

This is satisfied for ionization of all atoms in infrared fields of wavelength $\lambda \simeq 1\mu\text{m}$; for highly charged ions with I_p -s of several dozens eV and higher it is amply fulfilled. Condition (ii) means that the laser field is strong enough to generate a small relativistic drift of photoelectrons preventing they return to the parent ion and recollision. This happens for [57]

$$a_0 > \left(\frac{p_{\text{ch}}}{mc}\right)^{1/2} \left(\frac{E_0}{E_{\text{ch}}}\right)^{1/4} . \quad (2)$$

Here

$$a_0 = \frac{eE_0}{mc\omega} \quad (3)$$

is the celebrated dimensionless invariant field, E_0 is the electric field amplitude of the laser wave of frequency ω , e and m are the elementary charge and electron mass correspondingly, c is the speed of light. Finally, p_{ch} and E_{ch} are the characteristic electron momentum and electric field of the bound state.

When (1) is violated, particularly in the domain $\hbar\omega \simeq I_p$, the few-photon or single-photon ionization cross sections become generally complicated functions of the laser

frequency and may contain resonances. The ionization probability is no longer a monotonically decreasing function of I_p so that assumption II does not hold. In the high-frequency domain, $\hbar\omega \gg I_p$, several channels can compete including ionization of inner shells, ionization with excitation of the residual core and correlated double or multiple ionization by a single photon. This, assumption I also appears invalid.

When (2) does not apply, an electron removed from an atom through the single-electron ionization process, can return to this atom, provided the field is linearly or near to linearly polarized. This may cause recollision, a pivotal effect of nonlinear atomic optics responsible for the nonsequential double and multiple ionization [58], the generation of high order harmonics [59] and the high energy plateau in the photoelectron spectra [60]. For comprehensive review of the recollision physics we send the reader to Refs. [61–63]. For our subject, it is significant that the recollision can enhance the ionization probability of the second and the third electron by several orders in magnitude, the effect fully resulting from electron-electron correlations. In this situation the rate of doubly and triply charges ions production cannot be described within a single-electron sequential model. For $1\mu\text{m}$ wavelength light condition (2) satisfies for laser intensity $\mathcal{I} > 10^{16}\text{W}/\text{cm}^2$.

Summarizing this section, ionization can be introduced in PIC codes within a simple concept of a sequential single-electron process only for low-frequency fields (1) at intensities higher than $10^{16} - 10^{17}\text{W}/\text{cm}^2$ (2). For the most of the cases when PIC methods are used to simulate the dynamics of a laser-plasma interaction these requirements are satisfied. However, one has to notice that ionization of several outermost electrons in any atom happens at $\mathcal{I} < 10^{16}\text{W}/\text{cm}^2$. This means that it is hard to expect that this stage of the plasma formation will be correctly described in a PIC simulation. Fortunately enough, as we show below, formation of highly charged ions in intense fields is rather insensitive to the initial condition so that an incorrectly described initial stage of ionization will hardly influence the significant subsequent dynamics. Finally, inapplicability of the approach for description of ionization by high-frequency light means that the effect of secondary XUV and X-ray radiation emitted by the plasma on the production of ions remains entirely discarded.

III. ANALYTIC MODELS FOR SEQUENTIAL STRONG FIELD IONIZATION

In this section and below we use atomic units $e = m = \hbar = 1$ customary in nonlinear atomic optics and physics of strong-field ionization. In these units, the speed of light $c = 1/\alpha_e \approx 137$ with α_e being the fine structure constant. In atomic units, the electric and magnetic field strengths are scaled by the atomic electric field $E_{\text{at}} = m^2e^5/\hbar^4 = 5.14 \times 10^9\text{V}/\text{cm}$ and ionization poten-

tials – by the atomic energy $me^4/\hbar^2 = 27.2\text{eV}$. Ionization potential of atomic hydrogen is then $I_p(\text{H}) = 1/2$. Laser intensity is then expressed in the form

$$\mathcal{I} = E^2(1 + \rho^2)\mathcal{I}_{\text{at}},$$

$$\mathcal{I}_{\text{at}} = \frac{c}{8\pi} \frac{m^4e^{10}}{\hbar^8} = 3.51 \times 10^{16}\text{W}/\text{cm}^2, \quad (4)$$

where E is the electric field amplitude in atomic units and ρ is the ellipticity, $\rho = 0$ for linear and $\rho = \pm 1$ for circular polarization.

A. Tunneling ionization rates

Under condition (1), ionization of atoms and positive ions proceeds in a highly nonlinear regime, which was theoretically described within an analytic semiclassical approach pioneered by Keldysh [64] in the mid-60s [51, 65]. This approach also widely referred to as the Strong Field Approximation (SFA) was later developed in great details [66, 67]. For a comprehensive review of the Keldysh theory and SFA we send the reader to Refs. [54, 55].

Within the nonlinear regime, the type of ionization dynamics is determined by the value of the Keldysh parameter

$$\gamma = \frac{\sqrt{2I_p}\omega}{E_0} \quad (5)$$

with E_0 being the electric field amplitude. For $\gamma \ll 1$ ionization proceeds in the tunneling regime, when the laser field can be treated quasi-static, and the ionization probability is close to that in the static field. In the opposite multiphoton limit $\gamma \gg 1$ ionization can be treated as penetration of the electron through a rapidly oscillating barrier. This case is simple for analytic descriptions. However, ionization of higher charge states (starting from $Z = 3$) in optical and infrared fields always proceeds in the regime $\gamma \ll 1$ so that quasi-static field approximation can be safely used in a calculation of ionization rates.

In this limit, the rate of ionization of a level with orbital and magnetic quantum numbers l and m is given by

$$w^{\text{PPT}}(t) = 4C_{n^*l}^2 B_{l|m|} I_p \times \left(\frac{2}{F(t)} \right)^{2n^* - |m| - 1} \exp \left\{ -\frac{2}{3F(t)} \right\}, \quad (6)$$

$$B_{l|m|} = \frac{(2l+1)\Gamma(l+|m|+1)}{2^{|m|}\Gamma(|m|+1)\Gamma(l-|m|+1)}.$$

Here $n^* = Z/\sqrt{2I_p}$ is the effective principal quantum number, Z is the charge of the atomic residual (i.e. $Z = 1$ for the ionization of a neutral atom, $Z = 8$ for the ionization of a hydrogen-like neon ion, etc.), $Z \leq Z_m$,

where Z_m is the atomic number, and $\Gamma(x)$ is the Euler Gamma function. The dimensionless value

$$F(t) = \frac{E(t)}{E_{\text{ch}}}, \quad E_{\text{ch}} = (2I_p)^{3/2} \equiv \left(\frac{I_p}{I_p(H)} \right)^{3/2} \quad (7)$$

called *reduced electric field* is a ratio of the absolute value of the laser wave electric field to the characteristic field of the atomic level E_{ch} , with the former proportional to the atomic field introduced above. Finally, C_{n^*l} is the asymptotic coefficient of the single-electron wave function of the level at large distances from the ionic core [54]:

$$\psi_{n^*lm}(\mathbf{r}) \approx 2C_{n^*l} \sqrt{\kappa} (\kappa r)^{n^*-1} e^{-\kappa r} Y_{lm} \left(\frac{\mathbf{r}}{r} \right), \quad (8)$$

where $\kappa = \sqrt{2I_p}$ is characteristic momentum of the bound state. The rate (6) was derived by Perelomov, Popov and Terent'ev in 1966-67 [51–54] and is now universally referred to as the PPT rate. The derivations and comparisons with the experimental data and numerical results can be found in reviews [54, 55] and references therein.

The rate (6) is an approximation valid under the following conditions.

(a) Low-frequency field $\gamma \ll 1$ (5) and the multiquantum regime (1). Both of these requirements are amply satisfied for ionization in strong optical or infrared fields for intensities above 10^{16}W/cm^2 .

(b) Non-relativistic approximation. Although dynamics of free electrons becomes relativistic at $a_0 \simeq 1$ (3), and this stems to substantial relativistic effects in photoelectron spectra already for $\mathcal{I} \simeq 10^{17} \text{W/cm}^2$, the total ionization rate remains determined by non-relativist physics under the condition [49, 54]

$$\frac{2I_p}{3c^2} \ll 1. \quad (9)$$

According to estimates made in Ref. [49], the non-relativist approximation remains valid for the calculation of ionization rates up to intensities $\mathcal{I} \simeq 10^{25} \text{W/cm}^2$.

(c) The semi-classical approximation used to calculate the rate (6) applies when the electron energy $-I_p$ is well below the maximum of the potential barrier created by joint action of the Coulomb and the laser electric field so that the electron tunnels through a broad barrier of width $b \approx I_p/E(t)$ much greater than the De Broglie wavelength. This implies that [50, 54, 68–70]

$$E \ll E_{\text{BS}} = \frac{I_p^2}{4Z}. \quad (10)$$

Depending on the laser pulse duration and the value of the orbital quantum number l , the inequality (10) can be violated before the corresponding level is fully ionized (see the discussion and examples in [50]). This circumstance dictates the necessity to significantly correct the semiclassical PPT rate in the high-field domain of parameters. Models developed to extend the semiclassical

description to the barrier-suppression ionization (BSI) regime are discussed in the next subsection.

(d) Finally, the coefficient C_{n^*l} in Eqs. (6), (8) can either be found numerically within the Hartree-Fock or other self-consistent field approach [71, 72] or estimated using the asymptotic formula suggested by Hartree [73]:

$$C_{n^*l}^2 = \frac{2^{2n^*-2}}{n^* \Gamma(n^* + l + 1) \Gamma(n^* - l)}. \quad (11)$$

This approximation works generally well; see comparisons of this coefficient calculated by different methods for argon in Appendix A. However, Eq. (11) may fail for some neutrals and ions with small Z in p or d states. Generally, as one can see from the results of Appendix A, with good accuracy one may put $C_{n^*l}^2 = 1$ for all states.

In the tunnel ionization theory known in the literature as ADK [56], the orbital quantum number l in Eq. (11) is replaced by the effective orbital number $l^* = n^* - 1$. In the context of the ionization problem, this replacement (which solely distinguishes the ADK rate from the PPT one) does not seem to be justified. As one can see from the plot of Appendix A, it generally makes the agreement with the numerically found coefficient worse, except for several p -states with the lowest ionization potentials.

B. BSI regime

When the electric field of the laser wave approaches the value (10), the PPT formula (6) becomes progressively inaccurate, strongly overestimating the rate. Condition (10) can be rewritten in terms of the reduced field (7)

$$F \ll \frac{\sqrt{2I_p}}{16Z} = \frac{1}{16n^*}, \quad (12)$$

which shows that the applicability of the tunnel approximation breaks earlier for states with higher effective quantum numbers (see examples and discussion in the next subsection).

Different models have been suggested to estimate the rate of ionization in the domains $E \simeq E_{\text{BS}}$, $E > E_{\text{BS}}$ and $E \gg E_{\text{BS}}$. Here, we must emphasize two significant points. Firstly, in contrast to the semiclassical quasi-static domain specified by

$$F \ll 1, \quad \gamma \ll 1 \quad (13)$$

in the BSI regime no analytic methods exist capable of calculated the rate in the closed form (see e.g. [54] for further information). Thus, all analytic formulas for the rate known for this regime, although they assume some underlying physics, should be considered as interpolations. Secondly, with the reduced field F increasing, the rate of ionization increases fast, so that only the case $F < 0.2..0.3$ is of practical interest. If the laser intensity is so high that larger values of F can be achieved, the respective level will be stripped completely before the

field maximum. The respective estimates can be found in Ref. [49]. Thus, for calculation of ion yields in intense laser fields, one predominantly needs to use, apart from the main expression (6), its suitable extension into the domain of higher field, but still below E_{BS} .

Several methods are known for the interpolation of semiclassical ionization rates in the strong-field domain [54, 68, 74, 75]. Here we use the one suggested by Tong and Lin in [68]. It employs an empirical factor which suppresses the PPT rate with E approaching E_{BS} :

$$w^{TL} = w^{PPT} \exp\left(-\frac{\alpha}{8} \frac{E}{E_{BS}} n^*\right), \quad (14)$$

where α is a constant adjusted to fit the numerically calculated rate. For examples considered in [68] the best fit was achieved in the interval $\alpha = 6..9$, meaning that $\alpha n^*/8 \simeq 1 - 2$). The interpolation (14) works well for $E \lesssim E_{BS}$ [50, 68], but strongly underestimates the rate for $E > E_{BS}$ [69]. However, except for the case of strong laser pulses of extremely short duration, a level can not survive unionized up to $E > E_{BS}$ so that the extrapolation (14) as well as any other formula, which provides a numerically acceptable fit for $E \lesssim E_{BS}$, is sufficient for our purposes.

C. Hierarchy of quantitative inaccuracies

In this subsection, we list and briefly describe the main flaws of the scheme, which reduce its numerical accuracy. In Section V and Appendix A these flaws are examined numerically to demonstrate their impact on the results of PIC calculations.

1. Coefficients C_{n^*l}

The coefficients C_{n^*l} in (6), (8) can be found numerically within the Hartree-Fock or other appropriate model for many-electron atoms, while the asymptotic formula (11) and its modification used in [56] do not necessarily work well. The difference between the coefficients found numerically and the analytic asymptotic is demonstrated in Appendix A. The higher the effective quantum number n^* is, the better is the accuracy of (11), while for several first levels the difference in the factor $C_{n^*l}^2$ can reach almost an order of magnitude. The safest way to reduce this source of errors is to use numerically calculated coefficients, but this requires quite a considerable work to find them for all charge states of all elements. However, as we argued in Section II, ionization of several outermost can proceed nonsequentially so that it is hard to expect a correct result within the chosen model of ionization anyway. As ionization of these levels happens at relatively low intensities, this stage of the process is of marginal interest for most of the cases of laser-plasma interactions at high intensities simulated with PIC methods. Summarizing this point, we can state that using the Hartree

asymptotic (11) provides a good quantitative accuracy,¹ while the approximation suggested in [56] has no advantages for such calculations. We provide a version of the open-source code SMILEI [76] that implements the coefficients $C_{n^*l}^2$ in the approximation (11), or, alternatively, allows using the tabulated values for $C_{n^*l}^2$, for example, calculated by solving the Schrodinger equation for the electron asymptotic states [72].

2. Dependence on the magnetic quantum number m

The rate (6) depends on the value of the magnetic quantum number m quantized on the polarization direction of the electric field. The main $|m|$ -dependent factor $(2/F)^{-|m|}$ stems from the fact that for $m \neq 0$ the bound state wave function is zero in the polarization direction. Since quick tunnel ionization happens at $F = 0.03..0.05$ [49], the additional suppression factor is ≈ 0.02 for p -states with $m = \pm 1$. In other words, levels with $m = 0$ ionize much faster than the others. The m -connected ambiguity of the calculation comes from the fact that different models for population of the magnetic sub-levels can be applied. In the approach for PIC simulations, initially suggested by Nuter et al [23], it is assumed that all present electrons of p - or d -shells are distributed in m with equal probabilities. In this case the rate of ionization from an l -shell populated by $N \leq 4l + 2$ electrons in $Z - 1$ ion is²

$$\begin{aligned} w(Z, I_p, E(t), l) &= \frac{N}{2l + 1} \sum_m w(Z, I_p, E(t), l, m) \\ &\approx \frac{N}{2l + 1} w(Z, I_p, E(t), l, m = 0), \end{aligned} \quad (15)$$

where we used shorthand notation w for the ionization rate as a function of the listed parameters. Here we took into account that for $m = \pm 1$ and higher the probability of ionization is only few per cent of that for $m = 0$. This model assumes the presence of a small interaction which redistributes all the remaining electrons homogeneously in m after each ionization step. We do not see well justified arguments on what this interaction could be. As an alternative convenient for implementation in PIC codes, we suggest assuming that the m number is conserved. This can be justified to some extent by the fact that the magnetic field of the laser wave splits the sub-levels slightly so that their energies are not exactly equal and, in the presence of other interactions no transitions between sub-levels with different m happen. In

¹ As we mentioned, Eq. (11) may be inapplicable a neutral atomic state. This can be simply resolved by setting $C_{n^*l} = 1$ for this state, which does not break the adopted precision. See Appendix A for examples.

² We note that in the original work [23] the factor $N/(2l + 1)$ is not present. While it is typically ~ 1 (for p -electrons, it ranges from 1/3 to 2), it should be included for higher precision.

this case, the rigorous calculation appears quite cumbersome, but taking into account the m -suppression in the probabilities, one may simply assume that two electrons with $m = 0$ are being removed first, then sub-levels with $m = \pm 1$ are being ionized, etc. We implement this new procedure in SMILEI [76]. In Section V, we demonstrate and discuss numerical comparisons of these models for treating the dependence on m .

3. BSI regime

With the electric field of the laser wave growing relative to the barrier suppression field of the level (10) the semiclassical formula (6) becomes less accurate as it has been discussed in the previous subsection. This flaw is the most serious one of the whole scheme for there is no quantitatively accurate analytic expression for the rate beyond the semiclassical domain. However, the situation remains bearable mostly because it is difficult to reach high values of E/E_{BS} or F before the level is entirely ionized. In [49] the value of the reduced electric field was estimated, at which the level is ionized within a single optical period as $F_0 = 0.03..0.05$. Then, at this threshold

$$\frac{E}{E_{BS}} = 4F_0 n^* = (0.1-0.2)n^*, \quad (16)$$

which shows that the tunneling formula is less accurate for larger n^* . In particular, deviations from the semiclassical behavior and consequent numerical errors are higher for p and d states than for s states [50]. The formula of Tong and Lin [68] extrapolates the rate to the domain $E/E_{BS} = 0.1..0.5$, which is sufficient for calculations, as a population of an atomic level hardly survives the upper limit of this interval. In contrast, the formula derived by Kostyukov, Artemenko and Golovanov [45, 69]

$$w^{\text{KAG}} = \begin{cases} w^{\text{PPT}}(E), & E < E_1, \\ \alpha \frac{E}{Z}, & E > E_1, \end{cases} \quad (17)$$

extrapolates the rate to considerably stronger fields. Here the coefficient $\alpha \sim 1$ depends on the shape of the atomic potential (for the Coulomb potential $\alpha \approx 0.8$) and the threshold field $E_1 \sim E_{BS}$ is determined by the continuity of the rate. It corresponds to the lower root of the equation $w^{\text{PPT}}(E_1) = \alpha E_1/Z$. The expression for $E > E_1$ is obtained assuming the laser field much stronger than the atomic field and neglecting the electron kinetic energy with respect to its energy in the laser field. Though the extrapolation (17) works pretty well for $E \gg E_{BS}$, its implementation in PIC codes makes no effect on the ion yield as all ionization events happen at much lower fields $E < E_{BS}$ (at least as long as we consider the interaction with an incident laser pulse). The Tong-Lin formula (14) is included in the new implementation of SMILEI [76], while the rate from Eq. (17) is available in the version suggested by Ouatu et al [70].

4. Successive ionization of levels with close ionization potentials

Finally, the adopted scheme discards the possibility that levels with higher ionization potentials can be ionized before those with lower ionization potentials (see the second fundamental constraint in Section II). In the semiclassical domain, this assumption is in general well justified for the rate (6) as it drops quickly with increasing I_p due to the exponential factor. Exceptions may happen when two nearest ionization potentials are close in value. As an example, consider ionization of argon, the element we use to benchmark our calculations in this paper. In Ref. [77], the energy levels and spectra lines of argon are collected for all ionic states up to Ar^{17+} . Here we can find that one of the smallest relative difference in ionization potentials is for Ar^{13+} . While $I_p = 754$ eV for the outermost p -electron in the configuration $1s^2 2s^2 2p$, to remove a $2s$ electron from the same configuration one needs $\Delta I_p \approx 50$ eV more energy. Taking that ionization proceeds efficiently for $F \approx F_0 = 0.03..0.05$, we estimate that the probability to remove a $2s$ electron differs from the for the outermost $2p$ by factor $\exp\{-\Delta I_p/(I_p F_0)\} = 0.11..0.26$. This is a very important estimate which shows that the discard of multiple ionization pathways can introduce a greater error than three other factors described above. This also allows estimating the accuracy of the whole scheme to be on the level of 20 – 30%.³

IV. NUMERICAL IMPLEMENTATIONS

In a realistic scenario, atoms and ions interact with an incident laser pulse of finite duration. The amplitude of the field experienced by an atom or ion slowly increases on the time scales of the pulse envelope, meaning that (i) E in Eqs. (6), (14) depends on time, and (ii) electrons are stripped sequentially starting from outer shells. In order to determine the final ionization state, one has to apply some numerical procedure to quantitatively describe this dynamical process. So far, two basic numerical approaches have been suggested: rate equations [49, 50] and incorporation of ionization into PIC codes [2, 6, 19–23].

A. Rate equations

Within this approach one has to solve the set of rate equations

$$\frac{dn_Z}{dt} = \sum [n_{Z-1} w_{Z-1 \rightarrow Z} - n_Z w_{Z \rightarrow Z+1}], \quad (18)$$

³ We do not consider the impact of this issue in numerical examples in the current work, as its implementation in PIC codes can be challenging.

where $1 \leq Z \leq Z_m$, n_Z is the density of ions with charge Z and the summation is performed over all possible ionization pathways, see the details in [49]. Namely, non-sequential ionization can be included straightforwardly, and the dependence on the quantum numbers of each level can be accounted for rigorously.

The rate equations approach has certain limitations. Firstly, the number of equations in (18) is equal to Z_m and is large for the elements with the high atomic number, while the number of terms in the sum quickly grows with Z . Secondly, the ions motion as well as the plasma field are completely neglected. Finally, all other ionization mechanisms, e.g. collisional ionization, are abandoned and cannot be accounted for within this approach.

B. PIC simulations

An alternative approach is the incorporation of ionization into the PIC simulation loop [2, 6, 19–23]. At each timestep, the Monte Carlo procedure is applied for each macroparticle with charge Z ($0 \leq Z < Z_m$). If ionization occurs, a macroparticle is transformed to the one with charge $Z + 1$, a macroelectron is added to the simulation and the electromagnetic field loses energy [23, 78] spent on ionization. For better performance of the PIC scheme, the timestep typically amounts to a fraction of the field period. However, it can be still large when compared to the mean lifetime of one or more electronic bound states. The algorithm suggested by Nuter et al. [23, 31] resolves this issue by accounting for the possibility of several consecutive ionization events taking place within one timestep.

Realizations for PIC, including the multi-level ionization algorithm proposed in Ref. [23], follow the approximations given in Section II and, particularly, rely on sequential ionization of outermost electrons (i.e. the one having the lowest ionization potential I_p). This is equivalent to selecting only one path among all the possibilities, as compared to the rate equations (18). However, this path dominates as long as the conditions listed in Section II hold. The great advantage of the PIC approach is the possibility to study the effect of ionization on laser-plasma interaction, such as the injection of electrons for laser-plasma acceleration schemes [23], or interaction with neutral heavy atomic gas targets [70].

The algorithm of Nuter et al [23] suggests using a Monte-Carlo procedure that implements the tunneling ionization rates given in Eq. (6). The original implementation also relies on an additional simplification setting the magnetic quantum number m in Eq. (6) to zero for all electrons in the view of $w^{\text{PPT}}|_{m=0} \gg w^{\text{PPT}}|_{m \neq 0}$. As we discuss in Section III B, this approximation does not seem well justified, especially for rare plasmas.

Another additional assumption imposed in Ref. [23] is the replacement of the PPT rates given in (6) by the ADK formula, namely, by using the expression for the Hartree coefficient C_{n^*l} [see Eq. (11)] with l replaced by

$l^* = n^* - 1$. While the latter step is also not well justified, as we demonstrate in Section V and Appendix A, it does not significantly affect the calculations' precision.

C. Modified implementation for electronic states with $m \neq 0$

To improve the precision of the strong-field ionization description in PIC simulations of in a rare plasma, we implement a procedure accounting for an arbitrary value of $|m| \leq l$. We still assume that approximations listed in Section II (in particular, the sequential extraction) and that the tunneling formula (6) hold. In contrast to Ref. [23], we assume that m is conserved for electrons on the ion sub-shells. Since sub-levels sharing the same $|m|$ (at fixed l) have close ionization potentials, we assume that any of them can be extracted. This can be taken into account by introducing the degeneracy factor $g_{|m|}$ (namely, the number of residual electrons on the sub-shell) multiplying the rate (6).

The numbers m and $g_{|m|}$ are attributed to each electron as follows.

- I. Since $w^{\text{PPT}}|_{m=0} > w^{\text{PPT}}|_{|m|=1} > w^{\text{PPT}}|_{|m|=2} > \dots$, we assume that for electrons with the same l , the states with the lowest value of $|m|$ are ionized first.
- II. Electrons with the same l occupy the sub-shells in the order of increasing $|m|$ and for the same $|m|$ in the order of increasing m , see Tab. I for an illustration. For example, for the atomic configuration with 3 p -electrons ($l = 1$) in the outer shell, we choose $m = 0, 0, -1$ for these electrons.
- III. The PPT ionization rate is multiplied by the number of residual electrons $g_{|m|}$ on a sub-shell with a given value of $|m|$, see Tab. I for an illustration. For a full l -shell, this can be expressed by approximating the l.h.s. of Eq. (15) as follows:

$$\begin{aligned} w(Z, I_p, E(t), l) &= \frac{N}{2l+1} \sum_m w(Z, I_p, E(t), l, m) \\ &\approx 2w(Z, I_p, E(t), l, m=0) \\ &\quad + 4w(Z, I_p, E(t), l, |m|=1) + \dots, \end{aligned} \tag{19}$$

where we used $g_0 = 2$, $g_{|m|>0} = 4$.

In effect, knowing the atomic number A , we can assign a unique set of quantum numbers n^*lm and the factor $g_{|m|}$ to all electrons, and hence identify their extraction rate during successive ionization. To illustrate the process of quantum number assignment, we provide the sequence for ionization of neutral ^{12}Mg in Tab. II.

This scheme allows us to generalize the algorithm proposed by Nuter et al [23] simply by replacing the ionization rates therein, which does not reduce the code

performance. The corresponding new ionization module is available in SMILEI [76]. The suggested approach allows us to estimate the importance of accounting for $m \neq 0$ in PIC simulations. Let us note that heavy atoms with higher-order sub-shells such as d and f may require special treatment as the electronic sub-levels can have exceptional anomalies in their arrangement.

Table I. The order for electron successive extraction from a sub-level with fixed l at varying magnetic quantum number $|m| \leq l$ for ionization algorithm in PIC simulations.

Sub-level order	1	2	3	4	5	6	7	8	9	10	...
m	0	0	-1	-1	1	1	-2	-2	2	2	...
$g_{ m }$	2	1	4	3	2	1	4	3	2	1	...

V. NUMERICAL EXAMPLE: IONIZATION OF ARGON

Let us consider a particular example to illustrate the impact of the discussed approximations for tunneling ionization, the suggested approach to account for $m \neq 0$ electron states, and the BSI regime in PIC simulations. We use SMILEI [31] with a modified ionization module available on GitHub [76]. In particular, we implement the PPT rates as given by Eq. (6) with the coefficients C_{n^*l} either given by the Hartree approximation [see Eq. (11)], or within the ADK approach, or tabulated with arbitrary values. The dependence on m is included as described in Section IV C.

For this example, we consider the interaction of a short high-intensity laser pulse with a thin layer of initially neutral argon. The laser field is monochromatic at the wavelength $\lambda = 0.8 \mu\text{m}$ throughout. The pulse temporal envelope has the following shape:

$$f(t) = \begin{cases} \sin^2\left(\frac{\omega t}{2N_{\text{cyc}}}\right), & 0 \leq \omega t < 2N_{\text{cyc}}\pi, \\ 0, & \text{otherwise.} \end{cases} \quad (20)$$

where t is the time, ω is the laser frequency, and N_{cyc} is the total number of cycles in the pulse. Throughout, we set $N_{\text{cyc}} = 10$. The field propagates along the x -axis, and we assume that the linearly polarized electric field is directed along y -axis. Hence, the electric field components in the units of (3) read $\mathbf{E} = a_0 f(t) \{0, \cos(\omega t - kx), 0\}$,

Table II. Example of electron state arrangement and the ionization order for ^{12}Mg .

Shell	$3s$	$3s$	$2p$	$2p$	$2p$	$2p$	$2p$	$2p$	$2s$	$2s$	$1s$	$1s$
n	3	3	2	2	2	2	2	2	2	2	1	1
l	0	0	1	1	1	1	1	1	0	0	0	0
m	0	0	0	0	-1	-1	1	1	0	0	0	0
$g_{ m }$	2	1	2	1	4	3	2	1	2	1	2	1
Ionization order	1	2	3	4	5	6	7	8	9	10	11	12

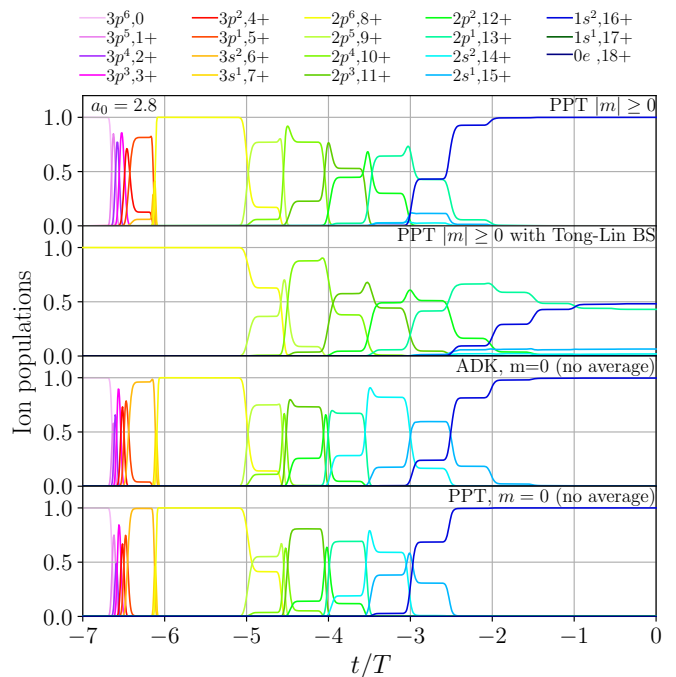


Figure 1. Evolution of ion populations in a thin initially neutral argon target (except the second plot, where initially Ar is charged to 8+) irradiated by a 10-cycle laser pulse for different tunneling ionization approximations in a 1D PIC simulation. The x -axis is shown in the units of field period $T = 2\pi/\omega$ and an ion population is defined as the ion density normalized to the initial neutral target density, n_Z/n_0 . The top plot shows the results obtained with the PPT rates calculated from Eqs. (6) and (11), combined with the suggested here approach to account for the electron states with non-zero m . In the second plot, we also use the Tong-Lin factor to study the impact of BSI [$\alpha = 6$, see Eq. (14)]. The two bottom plots correspond to the implementation suggested in Ref. [23], namely, $m = 0$ for all electrons, with the rates given by the ADK and PPT formulas, respectively [see Section III A]. Here, $a_0 = 2.8$ and the laser wavelength $\lambda = 0.8 \mu\text{m}$.

such that the wave and envelope maxima coincide. Here, $k = 2\pi/\lambda$ is the laser wavenumber in vacuum.

We keep the target density n_0 low so that collective effects are negligible. To be definite, in the simulations, we set $n_0 = 5 \times 10^{13} \text{ cm}^{-3}$, however, we will study only relative ion populations n_Z/n_0 for each ion with charge Z . The ionization process starts as soon as the laser pulse reaches the target. As we define as $t = 0$ the time at which the laser peak reaches the target, most ionization events happen at $t < 0$.

We perform 1D PIC simulation of this setup to study the ionization process dynamics and the dependence of the residual ion population on a_0 . The simulation box total length is 8λ , and the argon target occupies the 4 central cells. At the resolution 128 points per wavelength, this amounts to $\approx 0.03\lambda$. Such resolution was chosen as a result of convergence checks to ensure the simulation precision. We also choose 8192 particles per cell to

ensure high-quality statistics of the Monte-Carlo simulation of the ionization process. The results are presented in Figs. 1, 2, and also in Appendix A.

A. Ionization dynamics

Fig. 1 shows the ionization dynamics in the laser-target interaction at fixed field amplitude $a_0 = 2.8$. This value corresponds to the field that is slightly above the threshold of ionizing Ar^{15+} ($2s^1$ configuration), so that the final state is dominated by Ar^{16+} and the effect of the accounting for BSI correction on ionization of Ar^{15+} is clearly visible. The plot shows relative ion populations as a function of time for 4 ionization rate models: the one proposed in this work, which accounts for $m \neq 0$ electron states (first plot), the BSI Tong-Lin model (second plot), and the scheme previously proposed in Ref. [23] (two last plots). In all the cases, as the laser pulse edge reaches the target, the first levels (up to the $2p^6$ sub-level) are rapidly ionized. Apart from the BSI case (second plot), Ar^{16+} dominates in the final distribution.

Note that the PIC implementation additionally limits the applicability of the Tong-Lin model for BSI. Indeed, as we discussed above, Eq. (14) is valid for $E < E_{BS}$ and strongly underestimates the rate in the opposite case. For low I_p the field strength E can reach the BSI threshold E_{BS} (10) within one timestep, if the resolution of the simulation is not very high. It suppresses the ionization of low Z states, while in fact the outer electrons are stripped off at a very early stage of the interaction (see first plot in Fig. 1). To overcome this issue we assume that the target is partially ionized to some initial charged state $0 < Z^* < Z_m$ and consider $Z > Z^*$. In particular, we choose $Z^* = 8$ in the second plot of Fig. 1.

Let us compare our model (top plot in Fig. 1) to the scheme proposed in Ref. [23] (third plot, $m = 0$ for all e^- and the ADK formula is used).⁴ While the final states match, a detailed investigation shows differences in the ionization dynamics. Let us consider the $2p$ -shell. In the top plot, the ionization rate is suppressed by a factor of $2/F(t)$ at $|m| = 1$ [see Eq. (6)], hence, ionization of the p -states is retarded as compared to the third plot. At the same time, the ionization rate for s -states has no significant shift [recall that in our model the rate of $(l+1)s^2$ state ionization is multiplied by $g_0 = 2$ in contrast to Ref. [23]]. Notably, the $2s^1$ state almost does not appear in the top plot, as the $1s^2$ state rapidly dominates as the corresponding threshold field strength is reached. Note that the same features appear in the $3p$ - and $3s$ -shell ionization dynamics.

For the chosen value of the laser strength the effect of accounting for the BSI correction in the rates has noticeably stronger impact (see second plot in Fig. 1). The

ionization of $2p$ states happens considerably slower, and the final state mixes several ion species. This is the expected effect of barrier suppression, as the field strength is just above the threshold for the $1s^2$ state.⁵

We also test the PPT rate against the ADK approximation in the framework of Ref. [23]. As discussed in Section III A [see Eq. (11) and the follow-up explanations], they differ by the coefficient C_{n^*l} plugged in Eq. (6). The strongest distinction is noticed in the dynamics of the $2p$ -shell ionization, however, this difference is marginal as compared to the other cases discussed above. A more detailed comparison is presented in Appendix A.

B. Ion profiles

Figure 2a shows the residual ion populations as a function of the peak field strength (from now on referred to as the ion profiles). To obtain this data, we run a simulation for each value of a_0 to retrieve the ion population time dependence (as in Fig. 1), and take the final data point for each ion state. We use our model based on the PPT rate [Eqs. (6) and (11)] with account for $m \neq 0$ states as the benchmark, and subtract the second and the third plot from it to identify the difference explicitly, which is shown in Fig. 2b. Note that a relatively high difference can be seen for the outer shells corresponding to $l = 2$. However, the precision of all the models in this region is at the same level set by the general constraints discussed in Sections II and III C. Therefore, we will focus on the comparison of the results for deeper shells.

As one may expect, barrier suppression (second plot in Fig. 2a) leads to the overall shift of the ionization thresholds to higher fields. In particular, we reproduce the shift obtained for $1s$ states by Ciappina et al [50] by solving the rate equations. The strongest change can be noted for the $1s^2$ state threshold.

From the comparison of the first and the third plot in Fig. 2a, in the former, one can see the overall shift of the p -state ionization thresholds to higher fields. This comes from the ionization rate suppression for p -states with $|m| = 1$ in accordance with our approximation. For example, Ar^{10+} is predicted to dominate in the residual ion population for a wider interval of peak laser field intensities. At the same time, the model predicts that the populations of Ar^{14+} and Ar^{15+} are always marginal, as the threshold for $2p^1$ state shifts towards the $1s^2$ state, virtually suppressing the appearance of $2s^2$ and $2s^1$ states. Notably, such behavior is not seen in the third plot, the populations $2p$ and $2s$ shells alternate more regularly as the field strength is increased.

⁴ We also omit the prefactor $N/(2l+1)$ introduced in Eq. (15) for consistency with the original paper [23].

⁵ Note that the main purpose of this example is qualitative illustration. Here, we use the model parameter $\alpha = 6$, which, however, is not supported by any physical argument.

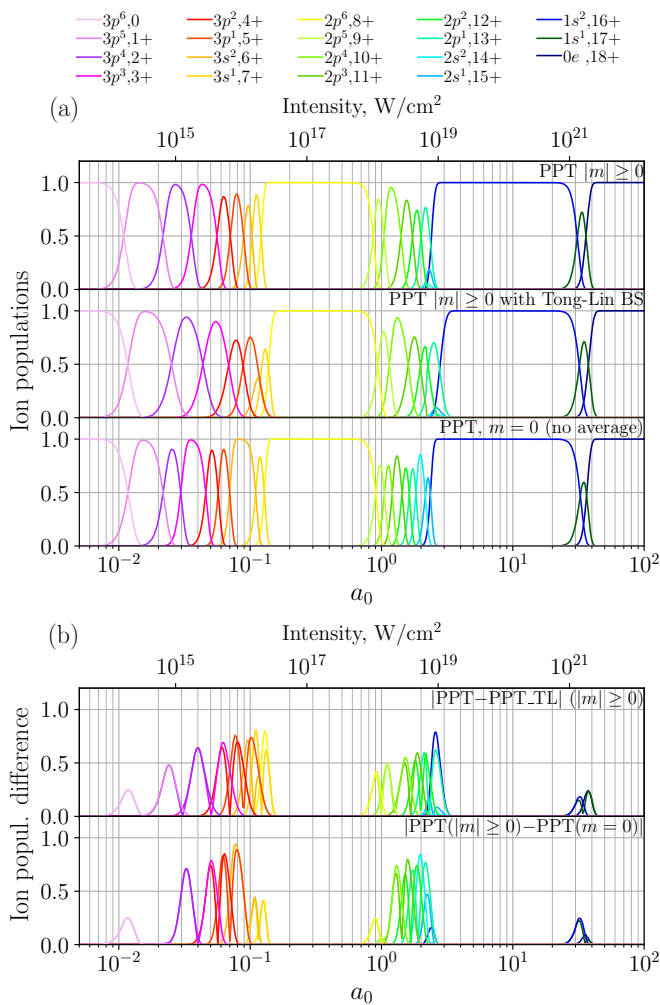


Figure 2. (a) Residual ion populations after the interaction of laser with the argon target as a function of the laser pulse peak field strength in the dimensionless units of a_0 (also shown in the units of intensity in the top horizontal axis) obtained from 1D PIC simulations. The notations are the same as in Fig. 1. (b) The absolute difference between the ion populations presented in panel (a). The curves for each ion state taken from the second and third plot in panel (a) are correspondingly (color-matched) subtracted from the curves in the top plot.

VI. CONCLUSION

To summarize, we discussed the aspects of strong-field ionization in PIC simulations in the context of laser-plasma interactions at high intensities. Although various analytic and numeric approaches to treat strong-field ionization have been developed for decades, the nature of the PIC method imposes strict constraints on the inclusion of the ionization process in simulation codes for practical applications. Although strong-field ionization is already included in many available PIC codes, in this work, we review the sources of possible inaccuracies and provide a refined model to treat this process in laser-plasma simulations. We illustrate the discussion with numerical ex-

amples obtained from the SMILEI PIC code [31] with the updated ionization module available on GitHub [76].

Strong-field ionization mainly applies to interactions with gas targets at very high intensities. The ionization rate for each atomic state can be deduced from the PPT theory [54], see Eq. (6), under the following hypotheses: (i) The ionization process is successive; (ii) Electrons occupy the lowest available level; (iii) The process takes place in the nonlinear regime $\gamma \ll 1$ so that the semi-classic approximation for electron dynamics is valid; (iv) Electrons are non-relativistic under the barrier. In practice, this means that Eq. (6) is applicable in the intensity range $\mathcal{I} \sim 10^{16}..10^{25}$ W/cm² (for optical lasers). Preferably, ions should also have some initial charge (e.g. $Z > 3$), however, this requirement can be omitted in many cases. In particular, assuming that a high-intensity laser pulse deeply ionizes atoms during the interaction, the outer shell electrons will be stripped off so quickly that the potential error in the calculation of their rates is negligible.

The implementation of the PPT formula (6) in PIC codes requires some additional assumptions. Firstly, the coefficients C_{n^*l} originating from the asymptotic electron wave-function (8) are usually approximated by the Hartree formula (11). It is common in PIC codes to use its simplified version with the reference to the ADK version of the PPT formula. While the latter step is not well-justified, and generally it is preferred to use Eq. (11) for better precision, this does not affect practical applications, at least for heavy atom ionization (as we illustrate in Section V in Appendix A).

A more noticeable discrepancy comes from the approximation required to treat the dependence on the magnetic quantum number m in Eq. (6) in the PIC method. While this issue is inherently connected to the successive ionization approximation, there are two visible ways of its consideration. In the first, following Ref. [23], m is simply set to zero for all states. However, this procedure does not seem to be well-justified, as the physical mechanism for transition between electronic states with $m \neq 0$ and $m = 0$ is not clear. We propose an alternative way, based on the assumption that the m -number is conserved for the inner electrons as the outer ones are stripped off. The main effect of the accurate treatment of m should be seen for the p , d and higher shells. At the same time, we do not see any noticeable change in the behaviour of s -shell electron ionization.

The account for states with $|m| > 0$ states results in the ionization rate suppression and hence the shift of the threshold field needed to ionize the given state. In effect, if the studied case of laser-plasma dynamics is sensitive to the ionization of these states, a refined treatment may change the results.

The ionization profiles are also affected in BSI regime [45, 50]. We adopted the Tong-Lin approximation [68] to identify its effect. In the considered examples, the ionization of p -shell appears to be as sensitive to this correction as to the account for $|m| > 0$ electronic states.

In the context of the proposed ionization-based techniques for measuring ultra-high laser intensities *in situ* [49, 50, 70], it means that p and higher electronic shells may be not the best option for gauging the field. While these states, potentially, can allow for high-precision measurements, it is first required to establish a well-tested ionization rate model for a reliable interpretation of the interaction outcome. On the other hand, ionization of s -shells is less affected by variation of the model, thus providing a more reliable basis for designing future experiments on ultra-high intensity measurement.

Overall, the highest source of potential errors originates from the hypothesis that the ionization process is successive. Outer electronic shells are the most sensitive to this issue, however, it should not be disregarded even for deeper shells with close values of I_p . In terms of the rate equations (18), it means that one has to account for multiple pathways of ionization. Partially, our model covers this issue, as we introduce the degeneracy factor for the states sharing the same $|m|$. However, a more rigorous treatment of possible pathways in PIC codes is required. Notably, the accurate treatment of many pathways is challenging for heavy atoms even within the rate equation approach. Hence, benchmarking of heavy-atom ionization in PIC codes is also problematic. This remains an important problem for future studies.

ACKNOWLEDGMENTS

This work was supported by Mobility plus project CNRS 23-12 from Czech Academy of Sciences and Centre national de la recherche scientifique, and by Sorbonne Université in the framework of the Initiative Physique des Infinis (IDEX SUPER).

Appendix A: Comparison of the approximations for the C_{n^*l} coefficients

Let us discuss the impact of choosing the value for the coefficients C_{n^*l} in the tunneling formula (6). Following the original approach [51–54], C_{n^*l} is the asymptotic coefficient of a single-electron wave function of the level at large distances from the ionic core, and cannot be found exactly analytically. Hence, it is suggested to use the Hartree approximation (11). In the ADK formula, this coefficient was simplified by replacing l with $l^* = n^* - 1$ (although the dependence on l in the $B_{|m|}$ in Eq. (6) is kept). As mentioned in Section III C 1, this can be a potential source of discrepancy, which we estimate here.

The coefficients C_{n^*l} can be extracted from matching the numerical solution

$$\psi_{nlm}^{HF}(\mathbf{r}) = \frac{P_{nl}(r)}{r} Y_{lm}\left(\frac{\mathbf{r}}{r}\right) \quad (\text{A1})$$

of the Hartree-Fock (HF) integro-differential equations with an exponentially decreasing solution (8) of the

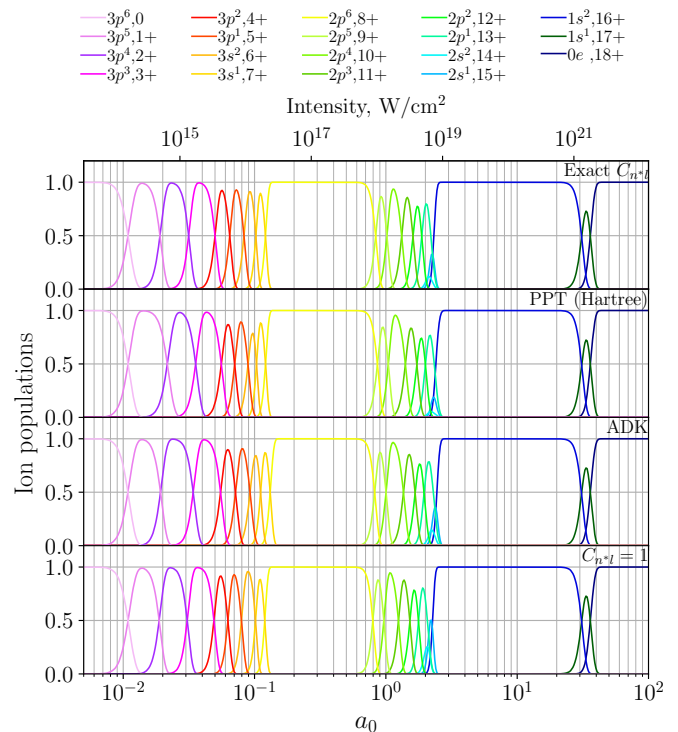


Figure 3. Ion profiles as a function of the laser pulse peak field strength in the dimensionless units of a_0 (also shown in the units of intensity in the top horizontal axis) obtained from 1D PIC simulations. In all simulations, we use the PPT formula (6) for the ionization rates with different approximations for C_{n^*l} : (first) exact values extracted from the asymptotic numerical solution to the Schrödinger equation, (second) Hartree formula (11), (third) ADK approximation [l is replaced by $l^* = n^* - 1$ in Eq. (11)], and (fourth) $C_{n^*l} = 1$ for all states. In all cases, we account for the dependence on m as described in Section IV C.

Schrödinger equation for the H-like ion with the charge Z at some point r_m [71, 72, 79, 80]. The main problem here is the optimal choice of the matching point r_m . On the one hand, the value of r_m must be large enough so that the radial HF function $P_{nl}(r)$ reaches the asymptotic with good accuracy, on the other hand, as r_m increases, the accuracy of the HF function $P_{nl}(r)$ calculation decreases.

Here the radial function $P_{nl}(r)$ has been obtained with a much higher accuracy than before [71, 72, 79, 80] by numerically solving the HF integro-differential equations using the finite difference method. Therefore, we were able to choose much larger value of the matching point r_m , precisely, where electron density $P_{nl}^2(r)$ is equal to 0.01 of its maximum value. We also verified that over a sufficiently wide range around the chosen r_m point, the constant C_{n^*l} remains unchanged by 4-5 significant digits.

The numerical values for C_{n^*l} obtained within different approximations are presented in Tab. III. We also calculate the relative error defined for given C_{n^*l} as

Table III. Coefficients C_{n^*l} and relative error Δ_{rel} (with respect to the calculated within different approximations for argon. $C_{n^*l}^{\text{exact}}$ is extracted from the numerical solution to the Schrodinger equation for asymptotic electron states.

Ion charge	Config.	$C_{n^*l}^{\text{exact}}$	$C_{n^*l}^{\text{Hartree}}$	Δ_{rel} Hartree	$C_{n^*l}^{\text{ADK}}$	Δ_{rel} ADK
0	$3p^6$	1.001	1.0*	0.001	1.016	0.015
1	$3p^5$	0.914	0.426	0.534	0.869	0.05
2	$3p^4$	0.842	0.534	0.366	0.724	0.14
3	$3p^3$	0.876	0.571	0.349	0.616	0.297
4	$3p^2$	0.772	0.581	0.247	0.513	0.335
5	$3p^1$	0.689	0.574	0.167	0.432	0.373
6	$3s^2$	0.954	0.906	0.051	0.428	0.551
7	$3s^1$	0.88	0.861	0.022	0.376	0.573
8	$2p^6$	0.652	0.513	0.214	0.764	0.172
9	$2p^5$	0.641	0.53	0.174	0.733	0.143
10	$2p^4$	0.633	0.542	0.144	0.707	0.115
11	$2p^3$	0.646	0.551	0.148	0.685	0.06
12	$2p^2$	0.634	0.56	0.117	0.658	0.039
13	$2p^1$	0.623	0.567	0.09	0.634	0.018
14	$2s^2$	1.043	1.021	0.021	0.624	0.402
15	$2s^1$	1.018	1.011	0.008	0.6	0.411
16	$1s^2$	1.003	0.994	0.009	1.005	0.002
17	$1s^1$	1.003	1.0	0.003	1.0	0.003

$\Delta_{\text{rel}} = |C_{n^*l}^{\text{exact}} - C_{n^*l}|/C_{n^*l}^{\text{exact}}$. Note that the first value for C_{n^*l} in the Hartree approximation (denoted with asterisk) is set manually, as Eq. (11) is not applicable to neutral atoms [Eq. (11) can take zero or even a complex value in this case]. This practical workaround allows us-

ing the Hartree approximation in PIC simulations. It should not affect the overall precision of calculations as long as strong fields and deep ionization states are considered.

As can be seen from the table, the relative error for the Hartree approximation is higher than that of ADK for the outer $3p$ -shell electrons. However, for deeper shells the Δ_{rel} becomes smaller for the former. Recall that the overall precision of the tunneling formula (6) is not that high for outer-shell electrons (see Section II). The lack of precision of Eq. (11) for such states is less important than the limitations imposed by the successive ionization approximation. Therefore, we conclude that as long as strong-fields ionization of deeper shells (in practice, $Z > 3$) is considered, the Hartree approximation is advantageous with respect to the ADK approximation for C_{n^*l} . Hence, usage of Eq. (11) in the PPT rate (6) is preferred unless a better approximation is available.

As a practical test, we calculate the ion profiles as in Section VB with different values for C_{n^*l} . The results are presented in Fig. 3. In addition to the three sets of C_{n^*l} listed in Tab. III, we also test a ‘‘poor man’s’’ approximation setting $C_{n^*l} = 1$. As can be seen from the plots, the results are very close. Slight difference can be seen in the $3p$ and $3s$ state profiles. The strongest deviation is seen for in forth plot, where the $2p$ state thresholds are shifted to the left. Overall, for practical applications, all the mentioned approximations for C_{n^*l} listed appear to be generally robust. For example, the refined treatment of the dependence on m has a higher impact on the model prediction.

-
- [1] C. K. Birdsall and A. B. Langdon, *Plasma physics via computer simulation* (CRC press, 2018).
- [2] T. Arber, K. Bennett, C. Brady, A. Lawrence-Douglas, M. Ramsay, N. J. Sircombe, P. Gillies, R. Evans, H. Schmitz, A. Bell, et al., Contemporary particle-in-cell approach to laser-plasma modelling, *Plasma Physics and Controlled Fusion* **57**, 113001 (2015).
- [3] A. Gonoskov, S. Bastrakov, E. Efimenko, A. Ilderton, M. Marklund, I. Meyerov, A. Muraviev, A. Sergeev, I. Surmin, and E. Wallin, Extended particle-in-cell schemes for physics in ultrastrong laser fields: Review and developments, *Physical review E* **92**, 023305 (2015).
- [4] J. M. Dawson, Particle simulation of plasmas, *Reviews of modern physics* **55**, 403 (1983).
- [5] A. Pukhov and J. Meyer-ter Vehn, Relativistic magnetic self-channeling of light in near-critical plasma: three-dimensional particle-in-cell simulation, *Physical review letters* **76**, 3975 (1996).
- [6] R. A. Fonseca, J. Vieira, F. Fiúza, A. Davidson, F. S. Tsung, W. B. Mori, and L. O. Silva, Exploiting multi-scale parallelism for large scale numerical modelling of laser wakefield accelerators, *Plasma Physics and Controlled Fusion* **55**, 124011 (2013).
- [7] T. Takizuka and H. Abe, A binary collision model for plasma simulation with a particle code, *Journal of computational physics* **25**, 205 (1977).
- [8] C. K. Birdsall, Particle-in-cell charged-particle simulations, plus monte carlo collisions with neutral atoms, *picmcc*, *IEEE Transactions on plasma science* **19**, 65 (1991).
- [9] K. Nanbu, Theory of cumulative small-angle collisions in plasmas, *Physical Review E* **55**, 4642 (1997).
- [10] F. Pérez, L. Gremillet, A. Decoster, M. Drouin, and E. Lefebvre, Improved modeling of relativistic collisions and collisional ionization in particle-in-cell codes, *Physics of Plasmas* **19** (2012).
- [11] Y. Sentoku, K. Mima, T. Taguchi, S. Miyamoto, and Y. Kishimoto, Particle simulation on x-ray emissions from ultra-intense laser produced plasmas, *Physics of Plasmas* **5**, 4366 (1998).
- [12] J. Vyskočil, O. Klimo, and S. Weber, Simulations of bremsstrahlung emission in ultra-intense laser interactions with foil targets, *Plasma Physics and Controlled Fusion* **60**, 054013 (2018).
- [13] B. Martinez, M. Lobet, R. Ducloux, E. d’Humières, and L. Gremillet, High-energy radiation and pair production by coulomb processes in particle-in-cell simulations, *Physics of Plasmas* **26** (2019).
- [14] I. V. Sokolov, N. M. Naumova, J. A. Nees, G. A. Mourou, and V. P. Yanovsky, Dynamics of emitting electrons in strong laser fields, *Physics of Plasmas* **16** (2009).
- [15] L. Sironi and A. Spitkovsky, Synthetic spectra from

- particle-in-cell simulations of relativistic collisionless shocks, *The Astrophysical Journal* **707**, L92 (2009).
- [16] M. Bussmann, H. Baur, T. E. Cowan, A. Debus, A. Huebl, G. Juckeland, T. Kluge, W. E. Nagel, R. Pausch, F. Schmitt, et al., Radiative signatures of the relativistic kelvin-helmholtz instability (2013) pp. 1–12.
- [17] R. Duclous, J. G. Kirk, and A. R. Bell, Monte carlo calculations of pair production in high-intensity laser–plasma interactions, *Plasma Physics and Controlled Fusion* **53**, 015009 (2010).
- [18] E. Nerush, I. Y. Kostyukov, A. Fedotov, N. Narozhny, N. Elkina, and H. Ruhl, Laser field absorption in self-generated electron-positron pair plasma, *Physical review letters* **106**, 035001 (2011).
- [19] B. Penetrante and J. Bardsley, Residual energy in plasmas produced by intense subpicosecond lasers, *Physical Review A* **43**, 3100 (1991).
- [20] P. Chessa, P. Mora, and T. M. Antonsen Jr, Numerical simulation of short laser pulse relativistic self-focusing in underdense plasma, *Physics of Plasmas* **5**, 3451 (1998).
- [21] D. L. Bruhwiler, D. Dimitrov, J. R. Cary, E. Esarey, W. Leemans, and R. E. Giacone, Particle-in-cell simulations of tunneling ionization effects in plasma-based accelerators, *Physics of Plasmas* **10**, 2022 (2003).
- [22] A. J. Kemp, R. E. Pfund, and J. Meyer-ter Vehn, Modeling ultrafast laser-driven ionization dynamics with Monte Carlo collisional particle-in-cell simulations, *Physics of Plasmas* **11**, 5648 (2004).
- [23] R. Nuter, L. Gremillet, E. Lefebvre, A. Lévy, T. Ceccotti, and P. Martin, Field ionization model implemented in particle in cell code and applied to laser-accelerated carbon ions, *Physics of Plasmas* **18** (2011).
- [24] M. Lobet, E. d’Humières, M. Grech, C. Ruyer, X. Davoine, and L. Gremillet, Modeling of radiative and quantum electrodynamics effects in pic simulations of ultra-relativistic laser-plasma interaction, *Journal of Physics: Conference Series* **688**, 012058 (2016).
- [25] L. Fedeli, A. Huebl, F. Boillod-Cerneux, T. Clark, K. Gott, C. Hillairet, S. Jaure, A. Leblanc, R. Lehe, A. Myers, et al., Pushing the frontier in the design of laser-based electron accelerators with groundbreaking mesh-refined particle-in-cell simulations on exascale-class supercomputers (IEEE, 2022) pp. 1–12.
- [26] F. Niel, C. Riconda, F. Amiranoff, R. Duclous, and M. Grech, From quantum to classical modeling of radiation reaction: A focus on stochasticity effects, *Phys. Rev. E* **97**, 043209 (2018a).
- [27] F. Niel, C. Riconda, F. Amiranoff, M. Lobet, J. Derouillat, F. Pérez, T. Vinci, and M. Grech, From quantum to classical modeling of radiation reaction: a focus on the radiation spectrum, *Plasma Physics and Controlled Fusion* **60**, 094002 (2018b).
- [28] C. S. Brady and T. Arber, An ion acceleration mechanism in laser illuminated targets with internal electron density structure, *Plasma Physics and Controlled Fusion* **53**, 015001 (2010).
- [29] S. Bastrakov, R. Donchenko, A. Gonoskov, E. Efimenko, A. Malyshev, I. Meyerov, and I. Surmin, Particle-in-cell plasma simulation on heterogeneous cluster systems, *Journal of Computational Science* **3**, 474 (2012).
- [30] H. Baur, R. Widera, W. Hönig, G. Juckeland, A. Debus, T. Kluge, U. Schramm, T. E. Cowan, R. Sauerbrey, and M. Bussmann, Picongpu: a fully relativistic particle-in-cell code for a gpu cluster, *IEEE Transactions on Plasma Science* **38**, 2831 (2010).
- [31] J. Derouillat, A. Beck, F. Pérez, T. Vinci, M. Chiaramello, A. Grassi, M. Flé, G. Bouchard, I. Plotnikov, N. Aunai, et al., Smilei: A collaborative, open-source, multi-purpose particle-in-cell code for plasma simulation, *Comput. Phys. Comm.* **222**, 351 (2018).
- [32] V. A. Vshivkov, N. M. Naumova, F. Pegoraro, and S. Bulanov, Nonlinear electrodynamics of the interaction of ultra-intense laser pulses with a thin foil, *Physics of Plasmas* **5**, 2727 (1998).
- [33] T. Liseykina and D. Bauer, Plasma-formation dynamics in intense laser-droplet interaction, *Physical Review Letters* **110**, 145003 (2013).
- [34] A. Gonoskov, T. Blackburn, M. Marklund, and S. Bulanov, Charged particle motion and radiation in strong electromagnetic fields, *Reviews of Modern Physics* **94**, 045001 (2022).
- [35] S. V. Popruzhenko, A. M. Fedotov, et al., Dynamics and radiation of charged particles in ultra-intense laser fields, *Uspekhi Fizicheskikh Nauk* **193**, 491 (2023).
- [36] A. Fedotov, A. Ilderton, F. Karbstein, B. King, D. Seipt, H. Taya, and G. Torgrimsson, Advances in qed with intense background fields, *Physics Reports* **1010**, 1 (2023).
- [37] Y. Azamoum, G. A. Becker, S. Keppler, G. Duchateau, S. Skupin, M. Grech, F. Catoire, S. Hell, I. Tamer, M. Hornung, M. Hellwing, A. Kessler, F. Schorcht, and M. C. Kaluza, Optical probing of ultrafast laser-induced solid-to-overdense-plasma transitions, *Light: Science & Applications* **13**, 109 (2024).
- [38] T. Hall, R. Hooper, N. Patel, and J. L. Pacheco, Tunnel ionization within a one-dimensional, undriven plasma sheath, *AIP Advances* **13**, 055315 (2023).
- [39] C. Bernert, S. Assenbaum, F.-E. Brack, T. E. Cowan, C. B. Curry, M. Garten, L. Gaus, M. Gauthier, S. Göde, I. Goethel, S. H. Glenzer, T. Kluge, S. Kraft, F. Kroll, M. Kuntzsch, J. Metzkes-Ng, M. Loeser, L. Obst-Huebl, M. Rehwald, H.-P. Schlenvoigt, C. Schoenwaelder, U. Schramm, M. Siebold, F. Treffert, T. Ziegler, and K. Zeil, Off-harmonic optical probing of high intensity laser plasma expansion dynamics in solid density hydrogen jets, *Scientific Reports* **12**, 7287 (2022).
- [40] P. Wang, Z. Gong, S. G. Lee, Y. Shou, Y. Geng, C. Jeon, I. J. Kim, H. W. Lee, J. W. Yoon, J. H. Sung, S. K. Lee, D. Kong, J. Liu, Z. Mei, Z. Cao, Z. Pan, I. W. Choi, X. Yan, C. H. Nam, and W. Ma, Super-heavy ions acceleration driven by ultrashort laser pulses at ultrahigh intensity, *Phys. Rev. X* **11**, 021049 (2021).
- [41] C. McGuffey, A. G. R. Thomas, W. Schumaker, T. Matsuoka, V. Chvykov, F. J. Dollar, G. Kalintchenko, V. Yanovsky, A. Maksimchuk, K. Krushelnick, V. Y. Bychenkov, I. V. Glazyrin, and A. V. Karpeev, Ionization induced trapping in a laser wakefield accelerator, *Phys. Rev. Lett.* **104**, 025004 (2010).
- [42] A. Pak, K. A. Marsh, S. F. Martins, W. Lu, W. B. Mori, and C. Joshi, Injection and trapping of tunnel-ionized electrons into laser-produced wakes, *Phys. Rev. Lett.* **104**, 025003 (2010).
- [43] B. B. Pollock, C. E. Clayton, J. E. Ralph, F. Albert, A. Davidson, L. Divol, C. Filip, S. H. Glenzer, K. Herpoldt, W. Lu, K. A. Marsh, J. Meinecke, W. B. Mori, A. Pak, T. C. Rensink, J. S. Ross, J. Shaw, G. R. Tynan, C. Joshi, and D. H. Froula, Demonstration of a narrow energy spread, ~ 0.5 GeV electron beam from a two-

- stage laser wakefield accelerator, *Phys. Rev. Lett.* **107**, 045001 (2011).
- [44] C. Thauray, E. Guillaume, A. Lifschitz, K. Ta Phuoc, M. Hansson, G. Grittani, J. Gautier, J.-P. Goddet, A. Tafzi, O. Lundh, and V. Malka, Shock assisted ionization injection in laser-plasma accelerators, *Scientific Reports* **5**, 16310 (2015).
- [45] I. I. Artemenko and I. Y. Kostyukov, Ionization-induced laser-driven QED cascade in noble gases, *Phys. Rev. A* **96**, 032106 (2017).
- [46] E. A. Chowdhury, C. Barty, and B. C. Walker, “nonrelativistic” ionization of the l-shell states in argon by a “relativistic” 10^{19} w/cm² laser field, *Physical Review A* **63**, 042712 (2001).
- [47] K. Yamakawa, Y. Akahane, Y. Fukuda, M. Aoyama, N. Inoue, and H. Ueda, Ionization of many-electron atoms by ultrafast laser pulses with peak intensities greater than 10^{19} w/cm², *Physical Review A* **68**, 065403 (2003).
- [48] A. Link, E. A. Chowdhury, J. T. Morrison, V. M. Ovchinnikov, D. Offermann, L. Van Woerkom, R. R. Freeman, J. Pasley, E. Shipton, F. Beg, et al., Development of an in situ peak intensity measurement method for ultraintense single shot laser-plasma experiments at the sandia z petawatt facility, *Review of Scientific Instruments* **77** (2006).
- [49] M. Ciappina, S. Popruzhenko, S. Bulanov, T. Ditmire, G. Korn, and S. Weber, Progress toward atomic diagnostics of ultrahigh laser intensities, *Physical Review A* **99**, 043405 (2019).
- [50] M. Ciappina and S. Popruzhenko, Diagnostics of ultraintense laser pulses using tunneling ionization, *Laser Physics Letters* **17**, 025301 (2020).
- [51] A. Perelomov, V. Popov, and M. Terent’ev, Ionization of atoms in an alternating electric field, *Sov. Phys. JETP* **23**, 924 (1966).
- [52] A. Perelomov, V. Popov, and M. Terent’ev, Ionization of atoms in an alternating electric field: II, *Sov. Phys. JETP* **24**, 207 (1967).
- [53] A. Perelomov and V. Popov, Ionization of atoms in an alternating electrical field. III, *Sov. Phys. JETP* **25**, 336 (1967).
- [54] V. S. Popov, Tunnel and multiphoton ionization of atoms and ions in a strong laser field (keldysh theory), *Physics-Uspekh* **47**, 855 (2004).
- [55] S. Popruzhenko, Keldysh theory of strong field ionization: history, applications, difficulties and perspectives, *Journal of Physics B: Atomic, Molecular and Optical Physics* **47**, 204001 (2014).
- [56] M. V. Ammosov, N. B. Delone, and V. P. Krainov, Tunnel ionization of complex atoms and of atomic ions in an alternating electromagnetic field, *Soviet Journal of Experimental and Theoretical Physics* **64**, 1191 (1986).
- [57] M. Klaiber, K. Hatsagortsyan, J. Wu, S. Luo, P. Grugan, and B. Walker, Limits of strong field rescattering in the relativistic regime, *Physical Review Letters* **118**, 093001 (2017).
- [58] M. Y. Kuchiev, Atonic antenna, *JETP lett* **45** (1987).
- [59] P. B. Corkum, Plasma perspective on strong field multiphoton ionization, *Physical review letters* **71**, 1994 (1993).
- [60] G. Paulus, W. Nicklich, H. Xu, P. Lambropoulos, and H. Walther, Plateau in above threshold ionization spectra, *Physical review letters* **72**, 2851 (1994).
- [61] F. Krausz and M. Ivanov, Attosecond physics, *Reviews of modern physics* **81**, 163 (2009).
- [62] W. Becker, X. Liu, P. J. Ho, and J. H. Eberly, Theories of photoelectron correlation in laser-driven multiple atomic ionization, *Reviews of Modern Physics* **84**, 1011 (2012).
- [63] W. Becker, S. Goreslavski, D. Milošević, and G. Paulus, The plateau in above-threshold ionization: the keystone of rescattering physics, *Journal of Physics B: Atomic, Molecular and Optical Physics* **51**, 162002 (2018).
- [64] L. Keldysh, Ionization in the field of a strong electromagnetic wave, *Sov. Phys. JETP* **20** (1965).
- [65] A. Nikishov and V. Ritus, Ionization of systems bound by short-range forces by the field of an electromagnetic wave, *Sov. Phys. JETP* **23**, 168 (1966).
- [66] F. H. Faisal, Multiple absorption of laser photons by atoms, *Journal of Physics B: Atomic and Molecular Physics* **6**, L89 (1973).
- [67] H. R. Reiss, Effect of an intense electromagnetic field on a weakly bound system, *Physical Review A* **22**, 1786 (1980).
- [68] X. Tong and C. Lin, Empirical formula for static field ionization rates of atoms and molecules by lasers in the barrier-suppression regime, *Journal of Physics B: Atomic, Molecular and Optical Physics* **38**, 2593 (2005).
- [69] I. Y. Kostyukov and A. Golovanov, Field ionization in short and extremely intense laser pulses, *Physical Review A* **98**, 043407 (2018).
- [70] I. Ouatu, B. Spiers, R. Aboushelbaya, Q. Feng, M. von der Leyen, R. Paddock, R. Timmis, C. Ticos, K. Krushelnick, and P. Norreys, Ionization states for the multipetawatt laser-qed regime, *Physical Review E* **106**, 015205 (2022).
- [71] A. A. Radzig and B. M. Smirnov, *Reference data on atoms, molecules, and ions*, Vol. 31 (Springer Science & Business Media, 2012).
- [72] N. Vitanov and G. Panev, On the asymptotic form of the electron wave function in the atom and the ion, *Europhysics Letters* **16**, 159 (1991).
- [73] D. R. Hartree, The wave mechanics of an atom with a non-coulomb central field. part i. theory and methods (Cambridge university press, 1928) pp. 89–110.
- [74] D. Bauer and P. Mulser, Exact field ionization rates in the barrier-suppression regime from numerical time-dependent Schrödinger-equation calculations, *Physical Review A* **59**, 569 (1999).
- [75] Q. Zhang, P. Lan, and P. Lu, Empirical formula for over-barrier strong-field ionization, *Phys. Rev. A* **90**, 043410 (2014).
- [76] A. Mironov, https://github.com/ArsenyMironov/Smilei_ionization.
- [77] E. B. Saloman, Energy levels and observed spectral lines of ionized argon, arii through arxviii, *Journal of Physical and Chemical Reference Data* **39** (2010).
- [78] S. Rae and K. Burnett, Detailed simulations of plasma-induced spectral blueshifting, *Physical Review A* **46**, 1084 (1992).
- [79] E. Clementi and C. Roetti, Roothaan-hartree-fock atomic wavefunctions: Basis functions and their coefficients for ground and certain excited states of neutral and ionized atoms, $z \leq 54$, *Atomic data and nuclear data tables* **14**, 177 (1974).
- [80] A. Evseev, A. Radtsig, and B. Smirnov, Asymptotics of wave-function of an electron in atom and ion, *OPTIKA I SPEKTROSKOPIYA* **44**, 833 (1978).